Biosynthesis of Copper Oxide-Silver Nanoparticles from Ephedra Intermedia Extract and Study of Anticancer Effects in HepG2 Cell Line: Apoptosis-Related Genes Analysis and Nitric Oxide Level Investigations

Nazanin Naderi, 🆔 **Azadeh Mohammadgholi*,** 🆔**Nastaran Asghari Moghaddam** 🆔

Department of Biology, Central Tehran Branch, Islamic Azad University, Tehran, Iran.

Article type:	**ABSTRACT**
Original Article	Liver cancer treatment faces significant obstacles such as resistance, recurrence, metastasis, and toxicity to healthy cells. Biometallic nanoparticles (NPs) have emerged as a promising approach to address these challenges. In this study, copper oxide-silver (Ag-doped CuO) NPs were prepared using a reduction method with *Ephedra* intermedia extract. The physicochemical properties of the NPs were evaluated using various techniques such as Field emission scanning electron microscopy (FESEM), Transmission Electron Microscope (TEM), X-ray diffraction (XRD), and Fourier-transform infrared spectroscopy (FTIR). Additionally, this study has evaluated nitric oxide levels (NO), reactive oxygen species (ROS) production, *Bax*, *Bcl2*, *P53*, and *Caspase3* genes expression, as well as cell viability within 24 hours in liver cancer cell line HepG2. FESEM and TEM imaging confirmed the nanostructural nature of the synthesized particles with sizes ranging from 31.27 to 88.98 nanometers. XRD analysis confirmed the crystal structure of the NPs. Comparative analysis showed that the IC_{50} values of the Ag-doped CuO NPs were significantly lower than that of the plant extracts. Molecular studies showed significantly increased expression of *Bax*, *Caspase3*, and *P53* genes, inducing apoptosis in cancer cells, and downregulation of *Bcl2* as a pro-metastasis gene. Additionally, the presence of Ag-doped CuO NPs significantly increased NO activity enzyme and ROS generation compared to the plant extract. The biosynthesized Ag-doped CuO NPs demonstrated the ability to induce apoptosis, increase ROS production, and enhance NO enzyme activity in HepG2 cancer cells, suggesting their potential as a therapeutic agent for liver cancer.

*Corresponding: Azadeh Mohammadgholi
Address: Department of Biology, Central Tehran Branch, Islamic Azad University, Tehran, Iran.
E-mail: a.mohammadgholi@yahoo.com

Introduction

Liver cancer is the sixth most common cancer and the third leading cause of death. Unfortunately, the global incidence of liver cancer is increasing at an alarming rate (1, 2). Despite significant advancements, conventional treatment approaches such as surgery, radiation therapy, chemotherapy, and hormone therapy face several challenges, including drug resistance, recurrence, metastasis, and toxicity to healthy cells (3, 4). Unfortunately, the global incidence of breast cancer is increasing at an alarming rate (5). Therefore, there is a great interest in investigating controlled drug release, targeted therapy, and decreasing adverse effects associated with anticancer drugs in cancer treatment (6, 7).In this context, the field of nanotechnology, which integrates knowledge from materials science, engineering, chemistry, biology, and medicine has opened up promising avenues in nanomedicine for the diagnosis, prevention, and treatment of cancer (8, 9). In the realm of diagnosis and prevention, the use of NPs in biosensors and their application in medical imaging have facilitated early detection and improved outcomes in cancer treatment (10, 11). Regarding cancer treatment, organic nanomaterials such as liposomes, polymers, dendrimers, and peptides have been extensively employed for the synthesis of NPs in medical applications due to their compatibility with living tissues (12-14). However, these NPs have practical limitations, including instability, premature drug release, rapid clearance, and susceptibility to immune responses (15, 16). As a result, mineral-based nanomaterials such as carbon nanostructures, silica NPs, and especially biologically active glasses and metal-based nanomaterials have gained attention as promising alternatives (17-20).

Metal NPs possess desirable properties for therapeutic delivery, including wide availability, abundant surface functionality, tissue compatibility, targeted delivery to cancer cells, and controlled drug release (21, 22). Additionally, the surface plasmonic properties of metal NPs enable simultaneous diagnostic and therapeutic applications, known as theranostics, thereby enhancing their utility in cancer treatment (23). From a therapeutic perspective, metal NPs have demonstrated efficacy in cancer treatment through mechanisms such as drug attachment, hyperthermia-induced cancer cell death, and modulation of autophagy and mitophagy processes in cancer cells (24).

In recent years, bimetallic NPs have attracted significant interest due to their superior physical and chemical properties compared to monometallic NPs (25). These bimetallic NPs' constituent metals have synergistic effects that enhance their biological properties, including antibacterial, optical, catalytic, electrical, thermal, and magnetic properties (26, 27). The emergence of the novel coronavirus disease (COVID-19) and increasing bacterial resistance are raising significant concerns (28). The potential of metal-based NPs effectively address these challenges lies in their antimicrobial properties (20).

Among various bimetallic NPs, copper oxide-silver (Ag-doped CuO) NPs have attracted attention due to its anticancer and antibacterial properties, making it a multifunctional NP with enhanced therapeutic potential (29). Although chemical methods have been originally used to synthesize these NPs, green synthetic approaches are gaining importance due to their environmental friendliness, cost-effectiveness, safety, and ease of synthesis (30, 31). For example, bimetallic Ag-doped CuO NPs are synthesized using Alternanthera sessilis (Linn). It showed remarkable anticancer properties against the HeLa cancer cell line. Moreover, these NPs have shown antibacterial activity against both Gram-negative and Gram-positive bacterial strains (32).

Considering the anticancer and antibacterial properties of *Ephedra* intermedia extract, it is a suitable choice for the biosynthesis of bimetallic Ag-doped CuO NPs. In this study, Ag-Cu NPs were prepared using a biogenic method using *Ephedra* intermedia extract. Their physical, chemical, and morphological properties were studied. Furthermore, its efficacy against the HepG2 liver cancer cell line was evaluated by analyzing NO enzyme levels, ROS, *Bax*, *Bcl2*, and *P53* gene expression, and cell viability.

Materials and methods

Trypsin-EDTA, trypan blue, medium RPMI-1640, fetal bovine serum (FBS), 3-(4,5-Dimethylthiazol-2-yl)-2,5-diphenyltetrazolium bromide (MTT), and penicillin/streptomycin 100 X were obtained from Gibco (ThermoFisher Scientific, USA). Merck (Germany) provided the Ag (NO3) and CuO (NO3) 2.6H2O. The Iranian Biological Resource Center (IBRC P1006547) provided the dried leaves of *Ephedra* intermedia. The HepG2 cell lines were acquired from the Pasteur Institute's Cell Bank in Iran. The annexin V/propidium iodide (PI), nitric oxide (ROS) assay, and DCFDA assay kits were provided by Roche (Germany). An 8-mm pores trans-well test kit was bought from Corning Life Sciences (USA). Tools utilized were the RevertAid First Strand cDNA Synthesis Kit (Lithuania) and the RNA Qiagen extraction kit (USA).

Ephedra intermedia leaf extract preparation

To produce the aqueous extract of *Ephedra* intermedia, the leaves were washed in distilled water and dried for 14 days at room temperature. The 0.3 g of dried *Ephedra* intermedia leaf was cooked for 10 minutes in 500 mL of purified water. The combination was then spun for 20 minutes at 5000 rpm using a Jouan-type centrifuge. Following a 10-minute microwave oven heating cycle at 540 W, the aqueous *Ephedra* intermedia extract was then kept at 4°C for further research.

Ag-doped CuO synthesis

To create Ag-doped CuO NPs, 80 mL of the extract was mixed with the necessary amount of CuO (NO3)2.6H2O (2.08 g /0.07 M) and 2.5 g of AgNO3. After being agitated for six hours at 140 degrees Celsius, the solution spontaneously cooled to ambient temperature. Then, the white sediment was collected by centrifugation for 10 minutes at 10,000 rpm. After that, the sediment was continuously washed with ethanol and distilled water (50/50 V/V) and allowed to dry overnight at 120 °C in a vacuum oven (33).

Characterization of biogenic Ag-doped CuO nanoparticles

The Ag-doped CuO NPs produced by biosynthesis were described using several techniques. An accelerating voltage of 15 kV, the FEI NOVA NANOSEM 450 Field emission scanning electron microscopy (FESSEM) and the Zeiss EM900 TEM (Transmission Electron Microscope) (Germany) were used to determine the shape and size of NPs. Ag-doped CuO NPs and *Ephedra* intermedia extract's molecular binding qualities, as well as the existence of key functional groups of phytochemicals were confirmed by Fourier-transform infrared spectroscopy, Spectrum Two, USA (FTIR). The area with wave numbers between 400 and 4000 cm−1 was scanned. The JSM-7500 FESSEM (Japan) in conjunction with an Energy Dispersive x-ray analyzer (EDX) was used to determine the elemental composition of biogenic Ag-CuO. X-ray diffraction (XRD) (PW3710, Netherlands) was used to determine the crystalline structure of *Ephedra* intermedia extract and Ag-doped CuO NPs (= 0.0260 nm). Using a Shimadzu-UV 1800 UV-Vis spectrometer and distilled

water as a reference, the absorption spectra of the synthesized sample (Ag-doped CuO NPs) were obtained in the region of 200-800 nm (33, 34).

Cell Cytotoxicity

Cancer cell cytotoxicity was assessed by MTT test. Briefly, the toxicity of both Ag-doped CuO NPs and *Ephedra* intermedia extricates was inspected after a 24-hour culture period utilizing the Calorimetric Strategy of 3-(4,5-dimethylthiazole-2-yl)-2,5-diphenyltetrazolium Bromide (MTT). Cells were cultured with *Ephedra* intermedia extricates and the Ag-doped CuO NPs (3.125, 6.25, 12.5, 25, 50 µg/ml) and incubated at 37°C and 5% CO2. At that point, after four hours of incubation with 100 µL of MTT solution, the crystals were dissolved in DMSO (Merck) and the amount of light absorption at 570 nm was determined using the Expert 96 microplate reader (Asys Hitch, Ec Austria). The cytotoxicity data were analyzed using the Pharm-PCS statistical package software to determine IC_{50} (34). The effect of toxicity of the Chemical synthesized Ag-doped CuO NPs and cisplatin on HepG2 cancer cells was also investigated. The toxicity of all samples was also evaluated on a certain healthy cell line.

Gene Expression

After 24 hours of exposure of HepG2 liver cancer cells to the IC_{50} of *Ephedra* intermedia extract and the Ag-doped CuO NPs, the levels of *Bax*, *Caspase3*, *P53*, and *Bcl2* in the cell cultures were assessed using qRT-PCR. RNA extraction was carried out with an RNeasy Plus Mini Kit (Qiagen), and cDNA synthesis was performed using an Easy cDNA Synthesis Kit (catalog number A101161). Real-time PCR analysis was employed to determine relative gene expression. Each PCR involved a 20 µL mixture of 13 Power SYBRH Green PCR Master Mix (ABI PRISM, 4368702), 12 ng cDNA, and specific primers. The designed primer sequences and reaction temperatures for each gene are presented in Table 1. The comparative method of 2-ΔΔCt was employed to analyze relative gene expression, with target gene Ct values normalized to *β-actin* and calibrated against untreated HepG2 cancer cells. At least three independent experiments were conducted for each test, and the assays were repeated using RiaGene6000 Qiagen (34).

Table 1. Sequence of primers and the size of the products used in the reaction

Genes	Primers
ß-actin	Forward: 5'- TCCTCCTGAGCGCAAGTAC-3' Revers: 5'- CCTGCTTGCTGATCCACATCT-3'
Bax	Forward: 5'- GAGCTGCAGAGGATGATTGC-3' Revers: 5'- AAGTTGCCGTCAGAAAACATG-3'
Bcl2	Forward: 5'- ATTGGGAAGTTTCAAATCAGC-3' Revers: 5'- CAGTCTACTTCCTCTGTGATGTTG-3'
P53	Forward: 5'- TAACAGTTCCTGCATGGGCGGC -3' Revers: 5'- AGGACAGGCACAAACACGCACC -3'
Caspase3	Forward:5'-CATACTCCACAGCACCTGGTTA-3' Revers: 5'-ACTCAAATTCTGTTGCCACCTT-3'

Flow cytometry

After determining the IC_{50} concentration of the respective treatment, HepG2 liver cancer cells were exposed to the IC_{50} concentration of the bio-synthesized Ag-doped CuO NPs and the plant extract for 24 hours. The cells were then washed with phosphate-buffered saline, and the sediment from the cell

centrifugation was treated with 200 μL of binding buffer, followed by the addition of 5 μL of Annexin V color and a 10-minute incubation at room temperature. The cells were washed with a binding solution, and 10 microliters of PI dye were introduced. Finally, flow cytometry (BD FACSCalibur Flow Cytometer, USA) was used to analyze the results.

Nitric Oxide (NO) Level

The Natrix kit was used to measure NO level. It utilizes the Griess technique to measure NO in biological samples such as serum, plasma, homogenous tissue, and cell lysates. The method indirectly evaluates the amount of NO by forming an azo dye through the reaction of sulfanilic acid with nitrite in an acidic solution, which can be measured in light absorption between 520 and 590 nm (Awareness Microplate Reader (Stat Fax 4200), USA) (23).

ROS Measurements

The H2DCFDA kit was utilized to assess the ROS generated by the extract and the doped NPs. This involved the reduction of dichlorodihydrofluorescein diacetate (DCFD) associated with cellular oxidation, producing 7`-dichlorodihydrofluorescein diacetate acetyl ester, which was then measured to detect the resulting oxidative stress. The highly sensitive HepG2 cell line was treated with the IC_{50} concentration for 24 hours. Following this, the cells were washed with buffered saline before being incubated with 80 mM H2DCFDA for 30 minutes at 37°C. Subsequently, the fluorescence intensity at 530 nm was measured using a microplate reader (Awareness Microplate Reader (Stat Fax 4200), USA) (34).

Process involves the incubation of leaf extract with silver nitrate ($AgNO_3$) and copper sulfate ($CuSO_4$) in distilled water, leading to a color change that indicates nanoparticle formation. Following centrifugation, the Ag-doped CuO NPs are purified. These biogenic nanoparticles are then taken up by cancer cells through endocytosis, where they exert significant anticancer effects. Transmission electron microscopy (TEM) and scanning electron microscopy (SEM) images confirm the internalization and morphology of the Ag-doped CuO NPs within the cancer cells. The nanoparticles induce apoptosis through multiple mechanisms, as evidenced by increased expression of pro-apoptotic genes (*P53*, *Caspase 3*, *Bax*) and decreased expression of the anti-apoptotic gene *Bcl2*. This genetic modulation leads to a significant increase in reactive oxygen species (ROS) production, which contributes to oxidative stress within the cancer cells, further promoting apoptosis. The Annexin V/PI staining analysis demonstrates the progression of cells through early and late apoptosis, as well as necrosis, confirming the potent anticancer efficacy of the Ag-doped CuO NPs. Reactive oxygen species (ROS) are chemically reactive molecules containing oxygen, such as superoxide anions (O_2^-), hydrogen peroxide (H_2O_2), and hydroxyl radicals (OH•). Under normal physiological conditions, ROS levels are tightly regulated by the cells' antioxidant defense systems. However, the introduction of Ag-doped CuO nanoparticles disrupts this balance, leading to an overproduction of ROS within cancer cells (Figure 1).

Data analysis

The data were analyzed using GraphPad Prism v.8. The data were presented as mean standard deviation (SD). To evaluate statistical significance, one-way ANOVA was employed, followed by Tukey post hoc. The level of statistical significance in all analyses was pre-set at = 0.05.
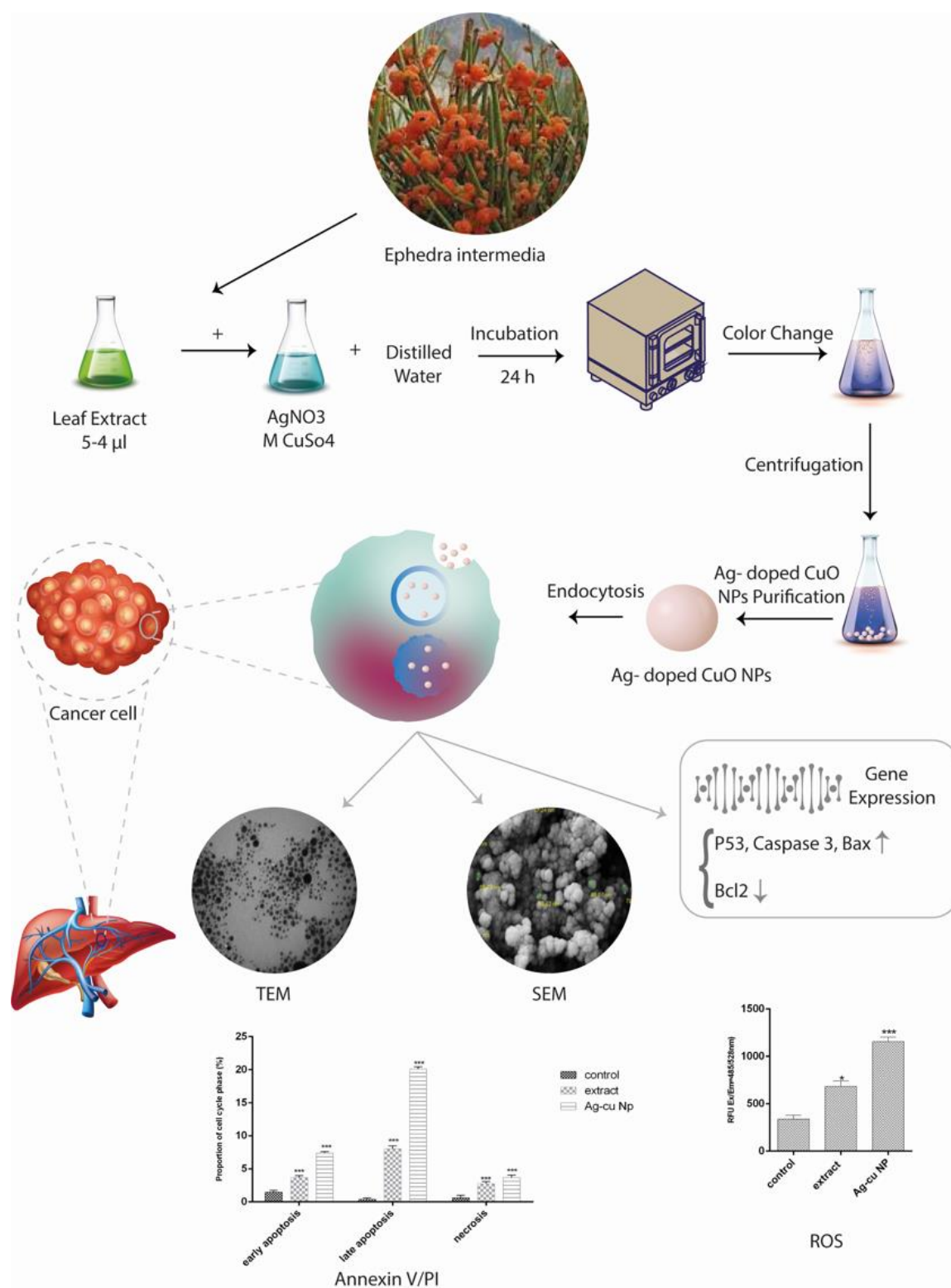
Fig. 1. This figure illustrates the synthesis of silver-doped copper oxide nanoparticles (Ag-doped CuO NPs) using *Ephedra intermedia* leaf extract, which acts as a reducing and stabilizing agent.

Results

Characterization of biogenic Ag-doped CuO nanoparticles

Using TEM and FESEM methods, the surface morphological properties of Ag-doped CuO bimetallic NPs derived from *Ephedra* intermedia extract were examined. The Ag-doped CuO NPs TEM and FESEM pictures are shown in Figures 2A and 2B, respectively. The FESEM picture shows adhesions and
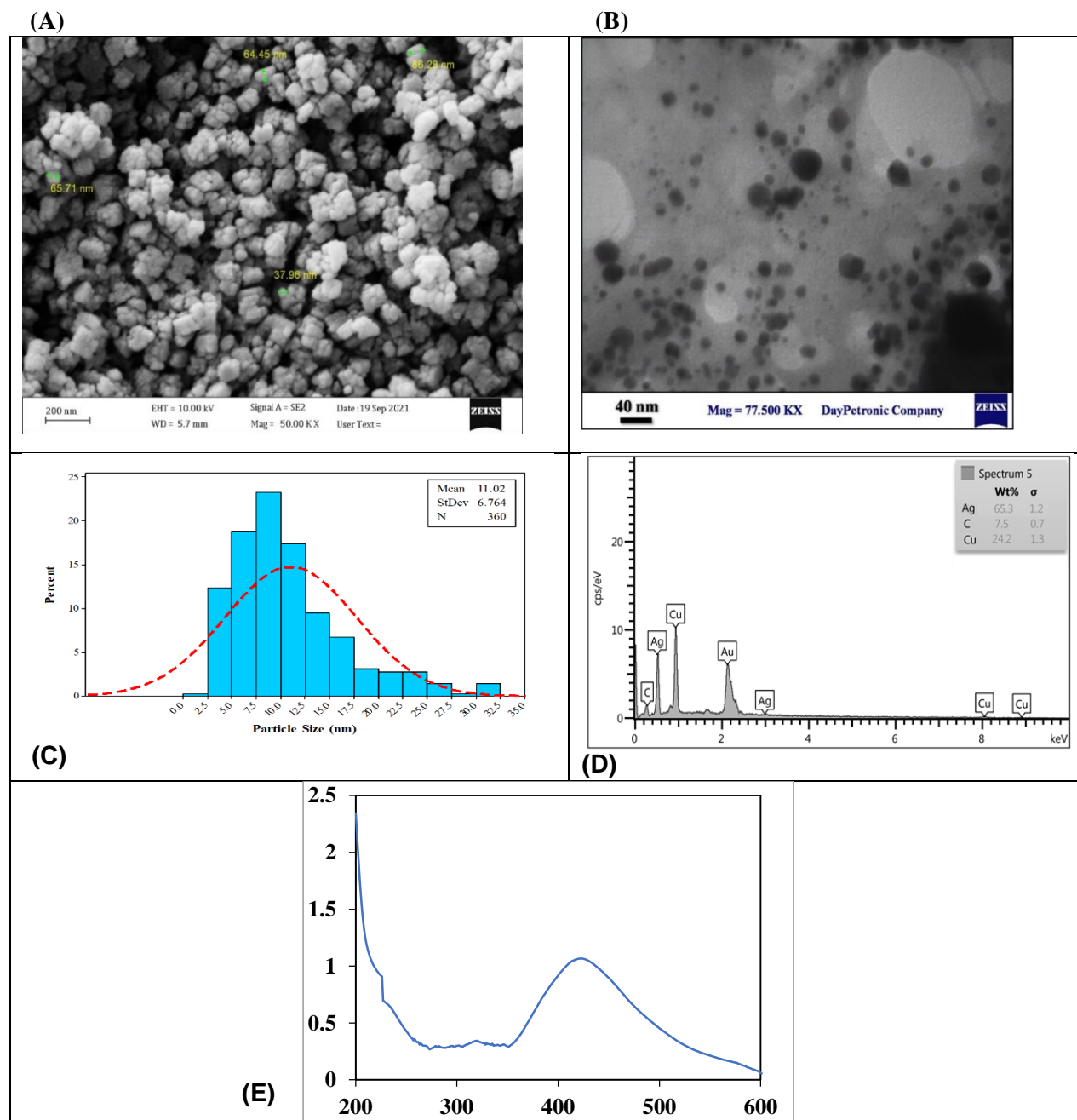
Fig. 2. A) Morphological characterization of doped biosynthesized Ag-doped CuO nanoparticles using (A) FSEM, (B) TEM, (C) size distribution of NPs (D) EDS tests, and (E) UV-Vis spectrum of Ag-doped CuO nanoparticles.

agglomerations among the Ag-doped CuO NPs that the plant extract produced. The Ag-doped CuO NPs were seen to exhibit agglomerations because of their tiny size (~50 nm). The morphology of Ag-doped CuO NPs was spherical, as may be shown. An in-depth examination of the morphology of Ag-doped CuO NPs was conducted by TEM analysis. The size and form of NPs may be precisely determined with the use of FESEM and TEM. The biosynthesized Ag-doped CuO NPs exhibited in Figures 2A and 2B, respectively, show the morphology and multi-layered, agglomerated surfaces along with their circular form. The size of the NPs ranges from 31.27 nm to 88.98 nm. The formation of biosynthesized NPs as agglomerates, with sizes varying and less than 40 nm, was also verified by TEM analysis. The average particle size was 12.02 nm, demonstrating the suitable and compact size of the produced Ag-doped CuO NPs.

To verify that the elements Ag, C, and Cu were present in the synthesized Ag-doped CuO NPs, an EDX examination was conducted using an extract from *Ephedra* intermedia. According to Figure 2C of the EDX method, the weight percentages of Ag, C, and Cu were 65.3%, 7.5%, and 24.2%, respectively. With the use of UV–visible spectroscopy, the stabilization of the biosynthesized Ag-doped CuO NPs is discovered. A large peak of about 430 nm in wavelength, as shown in this picture, suggests the presence of metal ions. This might be because plant extract reduces zinc and silver ions. According to the results of this test, *Ephedra* intermedia is a good stabilizing and reducing reagent for doped the Ag-doped CuO NPs synthesis. The UV-visible investigation indicated the presence of an absorption peak at 430 nm (Figure 2D). No another notable peak change was seen throughout responses and optimization.

The manufactured Ag-doped CuO NPs chemical groups were determined using the FTIR technique. The FTIR spectra of the Ag-doped CuO NPs and *Ephedra* intermedia are displayed in Figures 3A and 3B, respectively. These pictures show that the bands that appear at 1637 cm-1 and 3436 cm-1, respectively, are associated with OH stretching and C=O or C=C vibrations in the extract's structure. Additionally, the FTIR picture of the Ag-doped CuO NPs shows strong, distinct peaks in the range of 1123.26, 1452.30, and 2832.19 cm-1 that are associated with C-H plane bending vibration, CH3 symmetric bending, CH2 stretch vibrations, and OH stretch. Copper oxide pigment vibrations were seen at 661 cm-1 in the FTIR spectrum. It is possible that the carbonyl C=O group and the aldehyde stretching of the C-H bond are responsible for the absorption peaks that are present at 1609 and 2919 cm-1. There are a considerable number of hydroxyl (OH) groups in the structure, as shown by the strong peak in the 3431 cm-1 spot. The existence and interactions of the copper element are linked to the formation of many peaks in the 400–700 cm-1 range. The two XRD values were assigned many crystal planes, including (111), (200), and (220), based on the X-ray diffractor's detection of the biosynthesized Ag-doped CuO NPs XRD spectra. 35.70°, 52.61°, and 64.13° were the temperatures at which the products showed evidence of crystallinity (Figure 3C). The Ag-doped CuO NPs that were biosynthesized and showed a crystalline nature are seen in Figure 3C.

Cell Cytotoxicity

Cytotoxic impacts of the *Ephedra* intermedia extract and the Ag-doped CuO NPs on HepG2 cancer cells was considered. The extract and NP concentrations extended from 3.125 to 50 μg/mL and the MTT test was performed over 24 h. The data showed that as the concentrations of both extract and NPs are enhanced, the survival rate of cancer cells are significantly reduced. In particular, the Ag-doped CuO NPs revealed a noteworthy decrease in cell viability compared to *Ephedra* intermedia extract. Moreover, the difference in
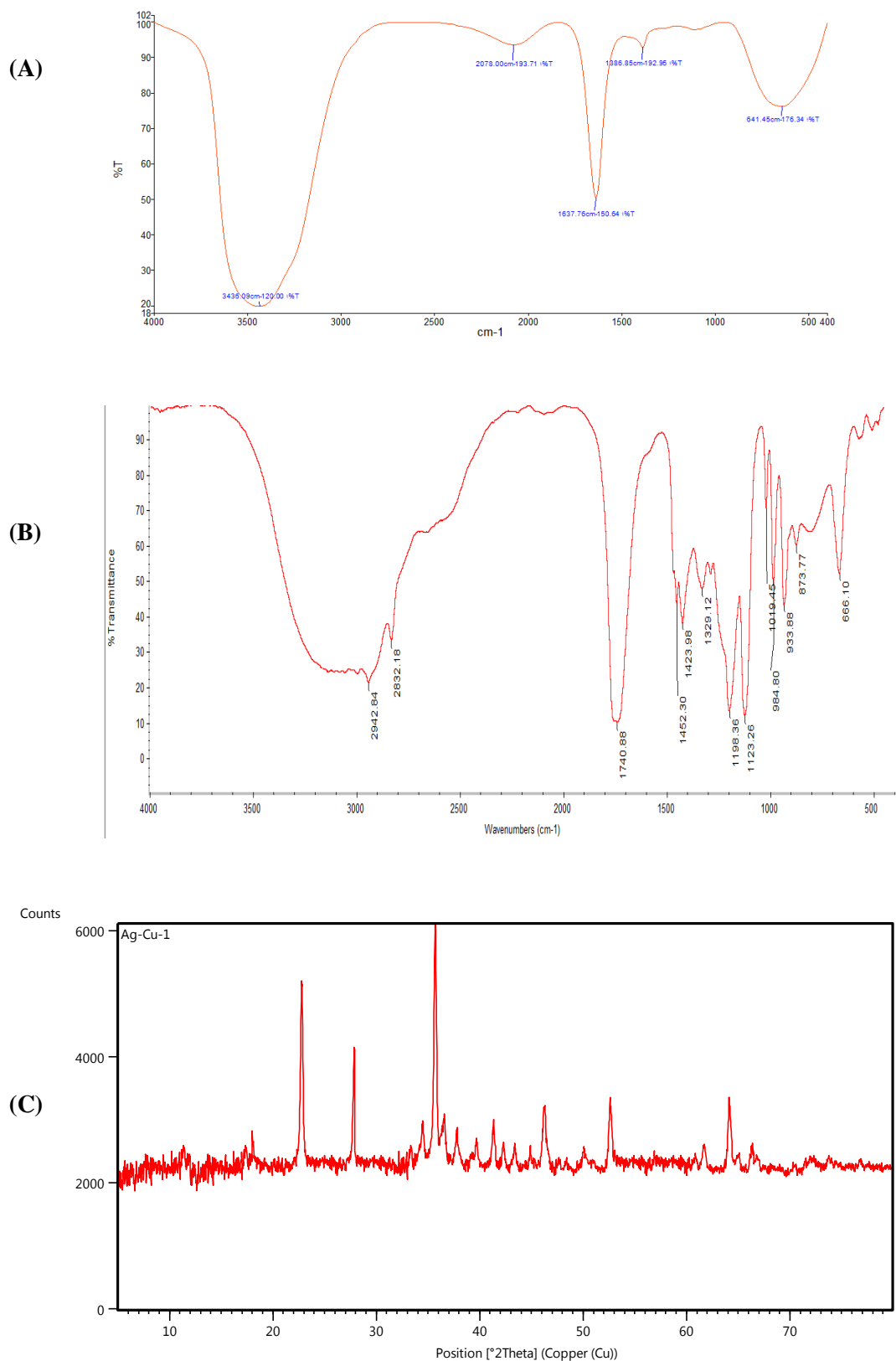
Fig. 3. (A) FTIR spectra of *Ephedra* intermedia extract, and (B) FTIR spectra of biosynthesized Ag-doped CuO nanoparticles. (C) XRD patterns of Ag-doped CuO nanoparticles.
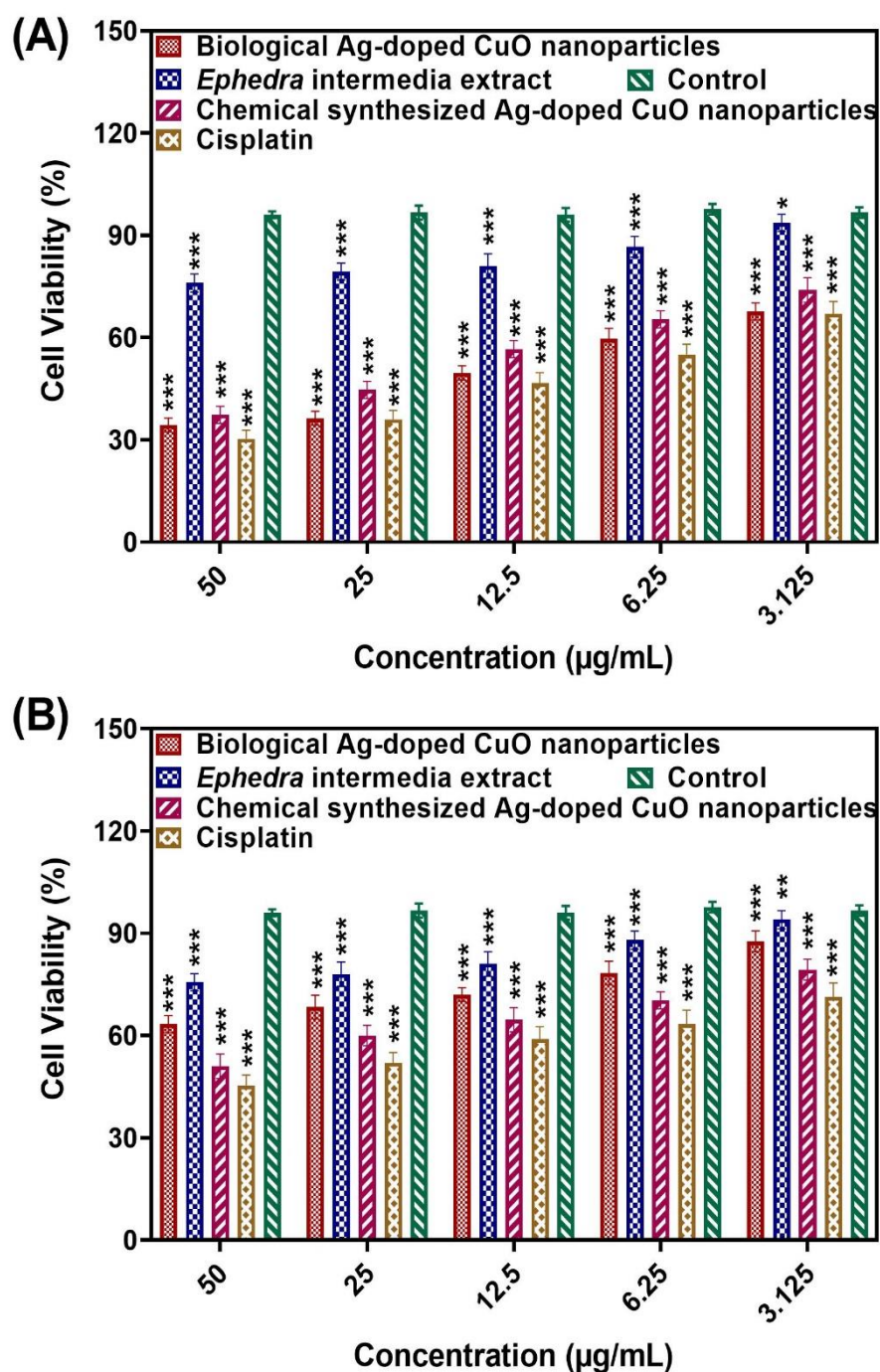
Fig. 4. **A)** The anticancer effects of *Ephedra* intermedia extract, cisplatin, biosynthesized Ag-doped CuO nanoparticles, and chemically synthesized Ag-doped CuO nanoparticles were evaluated at different concentrations (3.125 to 50 µg/ml) against the HepG2 liver cancer cell line over 24 hours using the MTT assay. The nanoparticles demonstrated significantly higher cytotoxicity against the cancer cells compared to the extract. **B)** The effects of *Ephedra* intermedia extract, cisplatin, biosynthesized Ag-doped CuO nanoparticles, and chemically synthesized Ag-doped CuO nanoparticles were evaluated at different concentrations (3.125 to 50 µg/ml) against the HFF healthy cell line over 24 hours using the MTT assay. * Indicates $P<0.05$, ** indicates $P<0.01$, and *** indicates $P<0.001$, signifying the level of statistical significance.

cell viability between the two treatments became more pronounced at higher concentrations. The HepG2 liver cancer cells displayed a critical decrease in viability at concentrations of 50 µg/ml (P<0.05) of the extract, as well as after treatment with the bio-synthesized NPs at concentrations extending from 6.25 to 50 µg/mL (P<0.001). These discoveries illustrate the anticancer impact of the synthesized NPs against liver cancer cells, even at low concentrations (Figure 4A). In this study, the IC_{50} values of both *Ephedra* intermedia extract and the synthesized Ag-doped CuO NPs were determined using the MTT assay. The IC_{50} value for the *Ephedra* intermedia extract was found to be 311.56 µg/mL, indicating the concentration at which 50% of the HepG2 liver cancer cells were inhibited. In contrast, the IC_{50} value for the Ag-doped CuO NPs synthesized by *Ephedra* intermedia was significantly lower, at 11.5 µg/mL. This drastic reduction in IC_{50} values demonstrates the enhanced cytotoxic efficiency of the NPs compared to the plant extract alone. This enhanced efficacy can be attributed to the unique physicochemical properties of the NPs, such as their small size, large surface area, and crystalline structure, which facilitate better cellular uptake and interaction with cancer cells. Also, we explored the cytotoxic impacts of the chemical synthesized Ag-doped CuO NPs and cisplatin on HepG2 cancer cells (Figure 4A). The MTT cell cytotoxicity assay against the HepG2 cancer cell line revealed distinct differences in the efficacy of the tested treatments. Across all evaluated concentrations, the biosynthesized Ag-doped CuO NPs and the chemically synthesized Ag-doped CuO NPs exhibited significantly higher cytotoxic effects than that of the *Ephedra* intermedia extract. However, the cisplatin demonstrated superior cytotoxicity relative to both types of NPs and the plant extract. Specifically, the cisplatin, the biosynthesized Ag-doped CuO NPs, and chemically synthesized Ag-doped CuO NPs consistently showed lower IC_{50} values (8.2 µg/mL, 11.5 µg/mL, and 14.1 µg/mL respectively), indicating higher potency in reducing cell viability. While the *Ephedra* intermedia extract had a moderate effect, it was less effective than both NP formulations (311.56 µg/mL).

The cytotoxicity assay on healthy cells indicated varying degrees of biocompatibility among the tested treatments. The biosynthesized Ag-doped CuO NPs exhibited the highest compatibility with healthy cells, showing the least cytotoxic effects (Figure 4B). This was followed by the chemically synthesized Ag-doped CuO NPs, which demonstrated moderate compatibility, and the *Ephedra* intermedia extract, which had slightly higher cytotoxicity. These results suggest that while the biosynthesized Ag-doped CuO NPs and the chemically synthesized Ag-doped CuO NPs are effective against cancer cells, they also maintain a favorable safety profile for healthy cells, making them potentially safer alternatives to conventional anticancer drugs.

Gene Expression

The alterations in the expression of apoptosis-promoting genes (*Bax*, *Caspase3*, and *P53*) and metastasis-related genes (*Bcl2*) in untreated cancer cells, as well as those treated with *Ephedra* intermedia extract and treated with the Ag-doped CuO Ns at their IC_{50} concentrations are shown in Figure 5. A significant increase in the expression of *Bax*, *Caspase3*, and *P53* genes was observed at the IC_{50} concentration, with approximately a 2.5 and 4-fold increase for the extract and the Ag-doped CuO NPs, respectively. Additionally, a notable decrease in *Bcl2* gene expression compared to the reference gene was evident. In general, it can be concluded that the Ag-doped CuO NPs have a more substantial impact on increasing the expression of pro-apoptotic genes and decreasing the expression of metastasis-stimulating genes than treatment with the *Ephedra* intermedia extract.
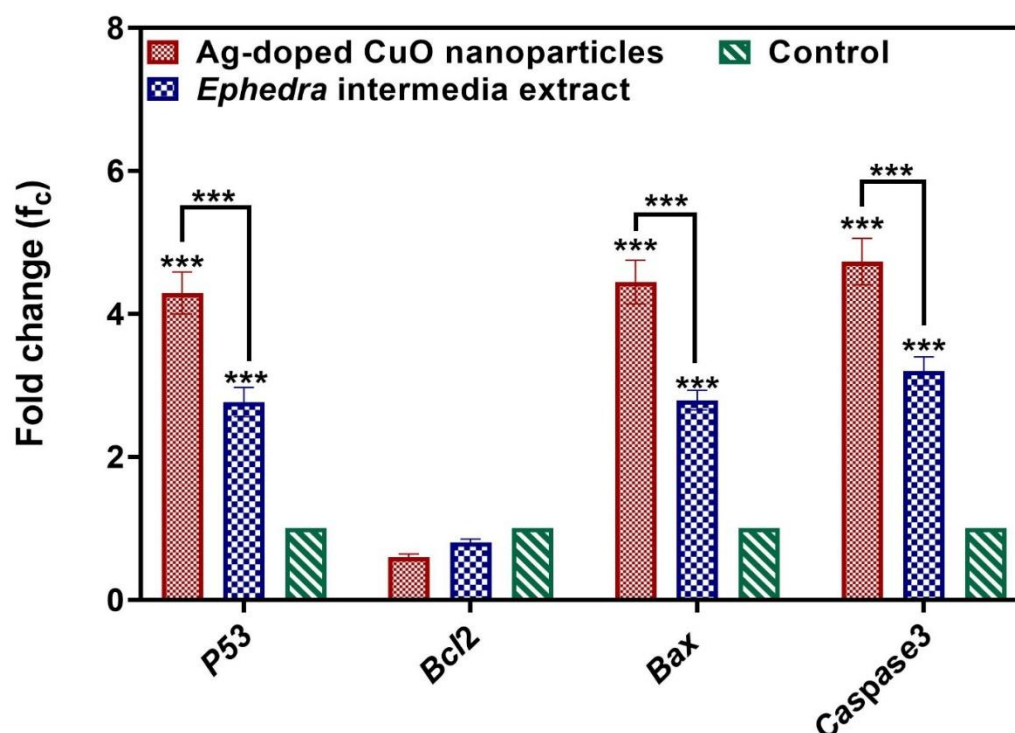
Fig. 5. Changes in the expression of *Bax*, *Bcl2*, *Caspase3*, and *P53* genes in HepG2 liver cancer cell line treated with the IC$_{50}$ concentration of *Ephedra* intermedia extract and Ag-doped CuO nanoparticles compared to the reference gene using Real-Time PCR technique. Compared to *Ephedra* intermedia extract, Ag-doped CuO nanoparticles have caused more increase in the expression of *Bax*, *Caspase3*, and *P53* genes as apoptosis promoters and a more severe decline in the expression of *Bcl2* as a metastasis promoter gene. * Indicates P<0.05, ** indicates P<0.01 and *** indicates P<0.001.

Flow cytometry

Figures 6A-C depict the occurrence of apoptosis and necrosis in the control cells (untreated), the cells treated with the extract, and the cells treated with the bio-synthesized Ag-doped CuO NPs at IC$_{50}$ concentrations. The assessment of cell cycle and apoptosis is crucial in evaluating the effectiveness of anticancer systems. According to these figures, 97.9% of the control cells remained viable. After treatment with the extract, respectively, 3.69%, 8.07%, and 2.79% of the cells entered the early and late apoptosis stages and underwent necrosis. Conversely, treatment with the Ag-doped CuO NPs resulted in 7.34% early apoptosis, 21.1% late apoptosis, and 3.77% necrosis in cancer cells. Additionally, Figure 6D demonstrates that the occurrence of both early and late apoptosis as well as necrosis in cells treated with both the extract and the Ag-doped CuO NPs was significantly higher than the control cells. Treatment with the Ag-doped CuO NPs led to approximately twice the occurrence of early and late apoptosis compared to cells treated with the extract (P<0.001).

Level of NO

Figure 7 reveals a significant increase in NO enzyme levels after treatment with the extract and the Ag-doped CuO NPs at IC$_{50}$ concentrations compared to the untreated control cells (P<0.05 and P<0.001, respectively). NO levels in the cells treated with the Ag-doped CuO NPs were approximately three times higher than that of the cells treated with the extract.

ROS Measurements

In this study, ROS levels was significantly increased after treatment with extracts and IC_{50} concentrations of the Ag-doped CuO NPs compared to the control cells (P<0.01 and P<0.001, respectively). As depicted in Figure 8, the increase in ROS levels in cells treated with the Ag-doped CuO NPs was approximately 1.5 times higher than in the cells treated with extracts. This finding aligns with the role of increased ROS levels in guiding cells toward programmed death, and the induction of nanoparticle-induced oxidative stress in cancer cells
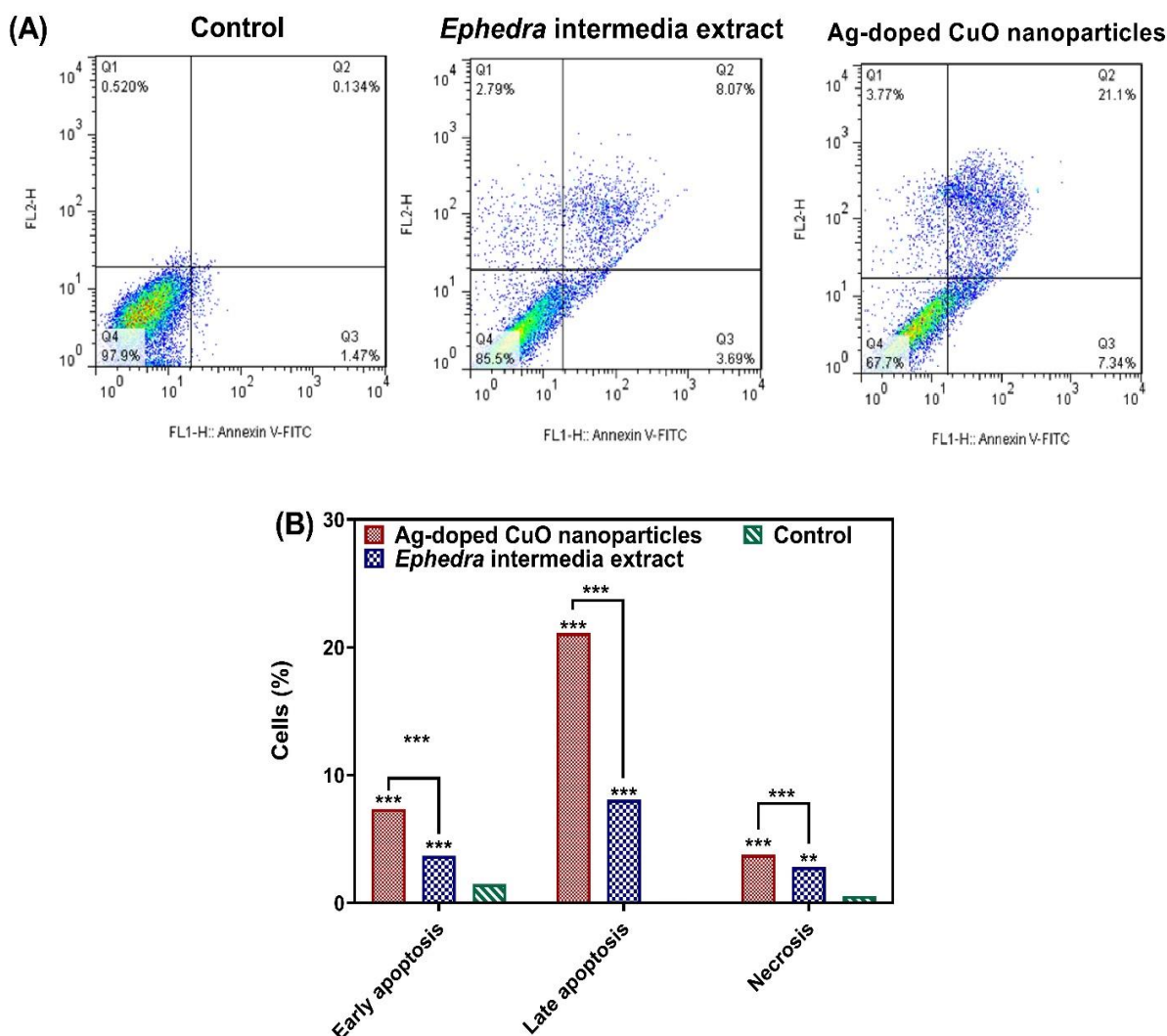

Fig. 6. Flow cytometry plot to assess early apoptosis and necrosis in A) control cells, B) cells treated with the IC_{50} concentration of *Ephedra* intermedia extract, and C) cells treated with the IC_{50} concentration of biogenic Ag-Cu nanoparticles. D) Changes in early apoptosis, late apoptosis, and necrosis in cells treated with the IC_{50} concentration of *Ephedra* intermedia extract and biogenic Ag-doped CuO nanoparticles compared to control cells using the flow cytometry technique. The observed increase in apoptosis and necrosis in the nanoparticle-treated group was significantly higher than in the extract-treated group. *** indicates P<0.001, indicating the level of statistical significance.
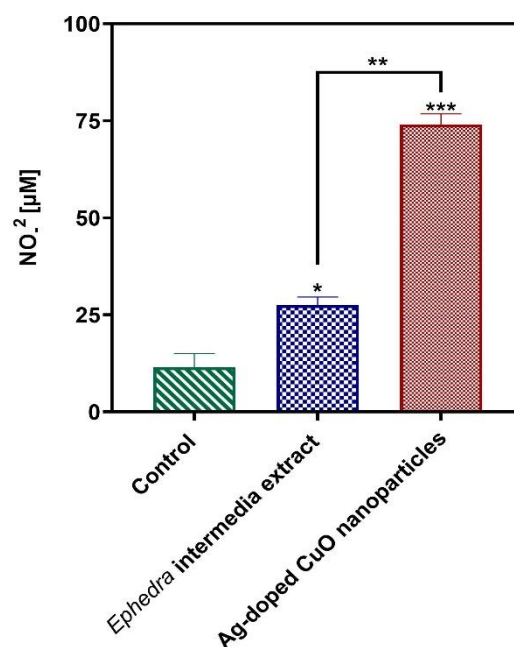
Fig. 7. The level of NO in cells treated with the IC$_{50}$ concentration of *Ephedra* intermedia extract and biogenic Ag-doped CuO nanoparticles compared to control cells. The observed NO concentration in the extract-treated group was approximately one-third of the concentration in the nanoparticle-treated cells. * Indicates P<0.05, and *** indicates P<0.001, indicating the level of statistical significance.

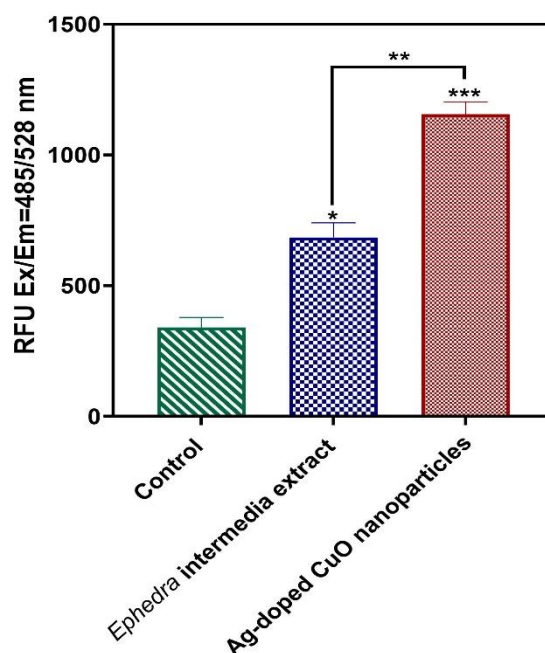**Fig. 8**. The production of ROS in cells treated with the IC$_{50}$ concentration of *Ephedra* intermedia extract and biogenic Ag-doped CuO nanoparticles compared to control cells. The observed ROS level in the nanoparticle-treated group was approximately 1.5 times higher than that in the extract-treated group. * Indicates P<0.05, and *** indicates P<0.001, indicating the level of statistical significance.

Discussion

The present study demonstrated that the biosynthesized Ag-doped CuO NPs using *Ephedra* intermedia extract exhibit significant anticancer effects on the HepG2 liver cancer cells. The biosynthesized Ag-doped CuO NPs was characterized by FESEM, TEM, XRD, and FTIR and showed a size range of 31.27 to 88.98 nanometers and a crystalline structure. Notably, these NPs exhibited a substantially lower IC_{50} value of 28.56 μg/mL compared to the plant extract's IC_{50} of 324.56 μg/mL, indicating a higher cytotoxic efficacy against the HepG2 cells. A noteworthy decrease in cell viability at concentrations as low as 6.25 μg/mL for NPs compared to higher concentrations required for the plant extract indicates the potent anticancer impact of the synthesized NPs even at low concentrations. Molecular analysis further substantiated the anticancer potential of the Ag-doped CuO NPs, with a significant upregulation of pro-apoptotic genes *Bax*, *Caspase3*, and *P53*, showing a 4-fold increase compared to a 2.5-fold increase with the plant extract. Conversely, the anti-apoptotic gene *Bcl2* was notably downregulated.

The data obtained from flow cytometry revealed that treatment with the Ag-doped CuO NPs resulted in a higher percentage of cells undergoing early and late apoptosis compared to the extract. This finding indicates that the Ag-doped CuO NPs have a more substantial impact on promoting apoptosis and reducing cell viability in liver cancer cells. Additionally, the study highlighted the ROS and NO in the anticancer mechanism of the NPs. Treatment with the Ag-doped CuO NPs significantly increased ROS levels and NO enzyme activity, approximately 1.5 times and three times higher, respectively, than the levels observed with the plant extract. This elevation in ROS and NO levels is critical in inducing oxidative stress and promoting apoptosis in cancer cells. Overall, these findings suggest that the biosynthesized Ag-doped CuO NPs from *Ephedra* intermedia extract exhibit a multifaceted anticancer mechanism, making them a promising therapeutic agent against liver cancer. ROS is linked to the eradication of cancer cells, measuring ROS levels a suitable indicator for evaluating anticancer activity. NO plays a crucial role in inhibiting tumor growth, angiogenesis, migration, and metastasis, making it a valuable indicator of the effectiveness of cancer treatments. Notably, the utilization of plant extracts has emerged as a promising avenue for liver cancer treatment, owing to their antioxidant and antiproliferative properties, coupled with reduced toxicity compared to conventional chemotherapy drugs (35, 36). A particular plant of interest in this regard is *Ephedra* intermedia, which has demonstrated significant anti-proliferative, anti-inflammatory, and antioxidant characteristics (37). Capitalizing on the advantages offered by NPs, particularly bimetallic NPs, incorporating the *Ephedra* intermedia extract in the synthesis of bimetallic Ag-doped CuO NPs appears to be a viable and advantageous strategy for cancer therapy (38).

The FESEM analysis, depicted in Figure 1A, illustrated spherical particles within the size range of 31.27 to 88.98 nanometers, while the Energy-Dispersive X-ray Spectroscopy (EDS) analysis, shown in Figure 1C, confirmed a silver content of 3.66% and copper content of 2.24%. The TEM image in Figure 1B further supported the observation of spherical nanoparticles with sizes below 80 nanometers, and the average particle size was calculated to be 11.20 nanometers, consistent with the findings reported by other researchers (39, 40). Furthermore, Fourier Transform Infrared (FTIR) spectroscopy results provided evidence of the presence of a carbon-carbon double bond, which contributes to the reduction of silver and copper ions (41).

In agreement with the FESEM data, the TEM picture indicates that the Ag-doped CuO NPs have spherical shapes and a non-uniform distribution. As reported by other research (42, 43), the results of the TEM picture further clearly show that the dark Ag particles are doped on the surface of CuO NPs. The aggregation of various NPs, which is not adequately done in the TEM diffraction microscope, and the NPs are observed stuck together, maybe the cause of the size disparity between the FESEM and TEM tests (41). The existence of improved dispersibility of Ag NPs in the nanorod-like morphology of CuO is confirmed by the Ag-doped CuO NPs cermet FESEM pictures. The face-centered cubic of Ag metal and the well-crystalline nature of monoclinic CuO were disclosed by XRD patterns, and the coating compositions were verified by EDX spectra (44).

The most identifiable ingredient is the primary synthesized (CuO and Ag) nanoparticle, according to a number of findings indicating that green synthesized CuO and Ag NPs have a spherical and nanoscale [31-33]. Ag and Zn have an absorption peak between 350 and 500 nm, as can be seen from the UV-Vis spectra of the other investigations (45, 46). Synthesized NPs are mostly caused by the participation of capping agents, which include amino acids, sugar, proteins, and dioica polysaccharides (47). CuO NPs were discovered to have UV spectra between 420 and 480 nm (48). Using UV-Vis-NIR and FTIR spectrophotometers, the optical characteristics of the produced coatings were examined in the wavelength ranges of 0.3–2.5 μm and 2.5–20 μm, respectively. At 700 rpm, the Ag@CuO Nanocermet coatings show an emissivity of ε=0.23 and a solar absorptance of α=0.93. Because the implanted Ag NPs contain concentrated free electrons with particle sizes that are either the same or smaller than the received light's wavelength, they improve the inherent absorption characteristics of CuO (44). The presence of four strong and four weak peaks indicated that the NPs were crystalline. The material's average crystallite size is directly correlated with the peak width in the XRD pattern. Typically, the size and crystallinity of the NPs are determined by sharp and wide peak regions. Ironically, XRD pattern of the biosynthesized NPs strikingly mimics the hexagonal silver wurtzite structure (49, 50). This supported the findings of earlier research (51, 52). Different extract secondary metabolites have been found on the outer layer of the doped NPs, as confirmed by the results of characterization techniques including UV-Vis, XRD, FTIR, and EDX tests. Essentially, Zn+ and Ag+ were converted into ZnNPs and AgNPs, respectively, by the action of flavonoids, amides, aromatic compounds, and amino acids found in the U. dioica extract as bio-reducing reagents (53). The combined benefits of including these specific chemicals on NP surfaces may increase the efficacy of Zn-doped-Ag NPs as apoptotic treatments.

Evaluation of the toxicity of the Ag-doped CuO NPs demonstrated notably higher toxicity compared to the *Ephedra* intermedia extract alone. The half-maximal inhibitory concentration (IC$_{50}$) of the NPs was significantly lower than that of the plant extract, aligning with the results reported by other researchers (54-57). The mechanism underlying the increased cytotoxicity of the Ag-doped CuO NPs involves multiple pathways. Firstly, the NPs induce oxidative stress by generating reactive oxygen species (ROS), which can damage cellular components and lead to apoptosis. Secondly, the NPs enhance the expression of pro-apoptotic genes such as *Bax*, *Caspase3*, and *P53* while downregulating the anti-apoptotic gene *Bcl2*. This gene expression profile promotes programmed cell death and inhibits cancer cell survival and proliferation (58). Among all tested agents, cisplatin exhibited the most pronounced cytotoxic effect, outperforming the

biosynthesized and chemically synthesized NPs as well as the *Ephedra intermedia* extract. The enhanced cytotoxic activity of the bimetallic NPs, both chemically and biosynthesized, can be attributed to their unique physicochemical properties. The small size, high surface area-to-volume ratio, and the synergistic effects of the metal components (silver and copper oxide) contribute to the improved cellular uptake and targeted delivery of the active compounds to the cancer cells. The biosynthesized Ag-doped CuO NPs, in particular, demonstrated superior cytotoxic efficiency, likely due to the additional benefits of the plant-derived capping and stabilizing agents that enhance the NPs' stability and biocompatibility (59, 60).

Elucidating the mechanisms underlying the heightened toxicity and induction of apoptosis at the IC_{50} concentration of both the extract and the synthesized NPs revealed a substantial upregulation of apoptosis-related genes, including *Bax*, *Caspase3*, and *P53*, accompanied by a downregulation of the anti-apoptotic gene *Bcl2*. Notably, the effect of the NPs on the upregulation of apoptosis-related genes and the downregulation of anti-apoptotic genes was more pronounced compared to the extract alone, which is consistent with findings from previous studies (61-64).

Furthermore, the evaluation of ROS and NO production, recognized as indicators of apoptosis induction and metastasis reduction, exhibited a significant increase in the presence of Ag-doped CuO NPs compared to the extract alone (65, 66). Given the central role of metastasis in the increased mortality associated with cancer, it is reasonable to anticipate that the synthesized NPs hold promise for future therapeutic applications (67).

Additionally, the analysis of cancer cells treated with NPs using flow cytometry revealed a substantial increase in apoptosis and necrosis compared to those treated with the *Ephedra* intermedia extract, corroborating the findings of this study and other investigations involving metallic NPs (32, 68). Collectively, these findings suggest that bimetallic Ag-doped CuO NPs synthesized using the *Ephedra* intermedia extract present a novel and promising therapeutic modality for liver cancer treatment.

The research findings suggest that Ag-doped CuO NPs can induce higher toxicity and apoptosis in cancer cells compared to *Ephedra* intermedia extract. The observed trends can be attributed to the different performance of extracts and NPs in inducing toxicity. It is thought that this extract has pharmacological functions similar to other drugs and may be able to cross the cell membrane wall due to its action on cell receptors or its concentration gradient (69, 70). However, the ability of NPs, due to their nano size, to easily penetrate the cell walls of cancer cells, leads to higher toxicity (71, 72). However, this mechanism can also cause relatively severe necrosis, which is undesirable (73, 74). The results of this research propose that modifying the surface of synthetic NPs with specific targeting agents could improve their performance in cancer treatment and detection. NPs have been shown to induce apoptosis in cancer cells through various mechanisms, such as ROS-mediated apoptosis and mitochondria-dependent apoptosis. Additionally, the use of NPs as drug delivery carriers shows potential for enhancing apoptosis in cancer cells. The findings highlight the potential of engineered NPs in cancer therapy and the importance of further research in this area (75-79).

Ag-doped CuO NPs were prepared using *Ephedra* intermedia extract. The physical characterization of NPs demonstrated that the Ag-doped CuO NPs had a higher small size and good uniformity. The cellular results also exhibited the high cytotoxicity of Ag-doped CuO NPs on HepG2 cells. Moreover, the Ag-doped

CuO NPs demonstrated a significant ability to induce apoptosis in liver cancer cells. The mRNA levels of pro-apoptotic genes (i.e., *Bax, Caspase3, P53*) increased; while the expression levels of cellular proliferative genes (*Bcl2*) decreased during treatment with NPs. The invasion of cells dramatically decreased after the treatment of the HepG2 cell line with biogenic Ag-doped CuO NPs. Therefore, as-designed green NPs had great potential for liver cancer treatment.

Acknowledgements

References

1. Toh MR, Wong EYT, Wong SH, et al. Global Epidemiology and Genetics of Hepatocellular Carcinoma. Gastroenterology 2023;164:766-82.

2. Foglia B, Turato C, Cannito S. Hepatocellular Carcinoma: Latest Research in Pathogenesis, Detection and Treatment. Int J Mol Sci 2023;24.

3. Anwanwan D, Singh SK, Singh S, et al. Challenges in liver cancer and possible treatment approaches. Biochim Biophys Acta Rev Cancer 2020;1873:188314.

4. Cadar R, Lupascu Ursulescu C, Vasilescu AM, et al. Challenges and Solutions in the Management of Hepatocellular Carcinoma Associated with Non-Alcoholic Fatty Liver Disease. Life (Basel) 2023;13.

5. Rumgay H, Arnold M, Ferlay J, et al. Global burden of primary liver cancer in 2020 and predictions to 2040. J Hepatol 2022;77:1598-606.

6. Hashemzaei M, Ghoshoon MB, Jamshidi M, et al. A Review on Romiplostim Mechanism of Action and the Expressive Approach in E. coli. Recent Pat Biotechnol 2024;18:95-109.

7. Schirrmacher V. From chemotherapy to biological therapy: A review of novel concepts to reduce the side effects of systemic cancer treatment (Review). Int J Oncol 2019;54:407-19.

8. Sedighi M, Mahmoudi Z, Abbaszadeh S, et al. Nanomedicines for hepatocellular carcinoma therapy: challenges and clinical applications. Mater Today Commun 2023;34:105242.

9. Bozorgpour R. Computational Explorations in Biomedicine: Unraveling Molecular Dynamics for Cancer, Drug Delivery, and Biomolecular Insights using LAMMPS Simulations. 2023; Available from: https://arxiv.org/abs/2311.13000.

10. Alimardani V, Rahiminezhad Z, DehghanKhold M, et al. Nanotechnology-based cell-mediated delivery systems for cancer therapy and diagnosis. Drug Deliv Transl Res 2023;13:189-221.

11. Park S, Cho E, Chueng SD, et al. Aptameric Fluorescent Biosensors for Liver Cancer Diagnosis. Biosensors (Basel) 2023;13.

12. Hosseini F, Mirzaei Chegeni M, Bidaki A, et al. 3D-printing-assisted synthesis of paclitaxel-loaded niosomes functionalized by cross-linked gelatin/alginate composite: Large-scale synthesis and in-vitro anti-cancer evaluation. Int J Biol Macromol 2023;242:124697.

13. Zaer M, Moeinzadeh A, Abolhassani H, et al. Doxorubicin-loaded Niosomes functionalized with gelatine and alginate as pH-responsive drug delivery system: A 3D printing approach. Int J Biol Macromol 2023;253:126808.

14. Salari N, Faraji F, Torghabeh FM, et al. Polymer-based drug delivery systems for anticancer drugs: A systematic review. Cancer Treat Res Commun 2022;32:100605.

15. Pedziwiatr-Werbicka E, Horodecka K, Shcharbin D, et al. Nanoparticles in Combating Cancer: Opportunities and Limitations. A Brief Review. Curr Med Chem 2021;28:346-59.

16. Awad NS, Salkho NM, Abuwatfa WH. Tumor vasculature vs tumor cell targeting: Understanding the latest trends in using functional nanoparticles for cancer treatment. OpenNano 2023;11:100136.

17. Amaldoss MJN, Yang JL, Koshy P, et al. Inorganic nanoparticle-based advanced cancer therapies: Promising combination strategies. Drug Discov Today 2022;27:103386.

18. Farmani AR, Nekoofar MH, Ebrahimi-Barough S, et al. Preparation and In Vitro Osteogenic Evaluation of Biomimetic Hybrid Nanocomposite Scaffolds Based on Gelatin/Plasma Rich in Growth Factors (PRGF) and Lithium-Doped 45s5 Bioactive Glass Nanoparticles. J Polym Environ 2023;31:870-85.

19. Ma J, Wang G, Ding X, et al. Carbon-Based Nanomaterials as Drug Delivery Agents for Colorectal Cancer: Clinical Preface to Colorectal Cancer Citing Their Markers and Existing Theranostic Approaches. ACS Omega 2023;8:10656-68.

20. Jin Y, Zhang F, Fan J, et al. A viable synthesis route of AgCu bimetallic nanoclusters on halloysite nanotubes and the study of the antibacterial properties. Applied Clay Science 2023;231:106750.

21. Liu C, Guo L, Wang Y. Delivering metal ions by nanomaterials: Turning metal ions into drug-like cancer theranostic agents. Coord Chem Rev 2023;494:215332.

22. Leong CY, Wahab RA, Lee SL, et al. Current perspectives of metal-based nanomaterials as photocatalytic antimicrobial agents and their therapeutic modes of action: A review. Environ Res 2023;227:115578.

23. Khorasani A, Shahbazi-Gahrouei D, Safari A. Recent Metal Nanotheranostics for Cancer Diagnosis and Therapy: A Review. Diagnostics (Basel) 2023;13.

24. Lei H, Pei Z, Jiang C, et al., editors. Recent progress of metal-based nanomaterials with anti-tumor biological effects for enhanced cancer therapy. Exploration; 2023: Wiley Online Library.

25. Makada H, Habib S, Singh M. Bimetallic nanoparticles as suitable nanocarriers in cancer therapy. Sci Afr 2023;20:e01700.

26. Shabatina TI, Vernaya OI, Shimanovskiy NL, et al. Metal and Metal Oxides Nanoparticles and Nanosystems in Anticancer and Antiviral Theragnostic Agents. Pharmaceutics 2023;15.

27. Mahmoodi Darian H, Bozorgpour R, Shafaee M. Numerical experiments on a hybrid WENO5 filter for shock-capturing. Numer Meth Part D E 2019;35:2375-406.

28. Farmani AR, Swanson RJ, Mahdavinezhad F, et al. Potential application of picosecond pulsed electric field (PPEF): advanced bioelectrical technology for potential COVID-19 treatment. J New Mater Electrochem Syst 2021;24:293-6.

29. Shamim MH, Kabir MF, Ferdousy J. Cost-Effective Biosynthesis and Characterization of Encapsulated Cu, Ag, and Magnetic Cu–Ag Bimetallic Nanoparticles for Biomedical Applications. BioNanoScience 2023;13:481-92.

30. El-Sheekh MM, AlKafaas SS, Rady HA, et al. How Synthesis of Algal Nanoparticles Affects Cancer Therapy? - A Complete Review of the Literature. Int J Nanomedicine 2023;18:6601-38.

31. Devi L, Kushwaha P, Ansari TM, et al. Recent Trends in Biologically Synthesized Metal Nanoparticles and their Biomedical Applications: a Review. Biol Trace Elem Res 2024;202:3383-99.

32. Babu H, Kareem MM, Lakshmi GV. Photocatalytic, antioxidant and biological activities of Alternantherasessilis (Linn.) leaf aqueous extract mediated ""'Ag-Cu"'" bimetallic nanoparticles. Mater Today Proc 2023.

33. Jadhav MS, Kulkarni S, Raikar P. Green biosynthesis of CuO & Ag–CuO nanoparticles from Malus domestica leaf extract and evaluation of antibacterial, antioxidant and DNA cleavage activities. New J Chem 2018;42:204-13.

34. Mirzaee Rad F, Tafvizi F, Noorbazargan H, et al. Ag-doped ZnO nanoparticles synthesized through green method using Artemisia turcomanica extract induce cytotoxicity and apoptotic activities against AGS cancer cells: an in vitro study. J Nanostructure Chem 2023:1-16.

35. Memarzia A, Saadat S, Asgharzadeh F, et al. Therapeutic effects of medicinal plants and their constituents on lung cancer, in vitro, in vivo and clinical evidence. J Cell Mol Med 2023;27:2841-63.

36. Singh AK, Singh SV, Kumar R, et al. Current therapeutic modalities and chemopreventive role of natural products in liver cancer: Progress and promise. World J Hepatol 2023;15:1-18.

37. Tang S, Ren J, Kong L, et al. Ephedrae Herba: A Review of Its Phytochemistry, Pharmacology, Clinical Application, and Alkaloid Toxicity. Molecules 2023;28.

38. Sharma G, Kumar A, Sharma S, et al. Novel development of nanoparticles to bimetallic nanoparticles and their composites: A review. J King Saud Univ Sci 2019;31:257-69.

39. Tantawy HR, Nada AA, Baraka A, et al. Novel synthesis of bimetallic Ag-Cu nanocatalysts for rapid oxidative and reductive degradation of anionic and cationic dyes. Appl Surf Sci Adv 2021;3:100056.

40. Biresaw SS, Taneja P. Copper nanoparticles green synthesis and characterization as anticancer potential in breast cancer cells (MCF7) derived from Prunus nepalensis phytochemicals. Mater Today Proc 2022;49:3501-9.

41. Ismail M, Khan MI, Khan SA, et al. Green synthesis of antibacterial bimetallic Ag–Cu nanoparticles for catalytic reduction of persistent organic pollutants. J Mater Sci Mater Electron 2018;29:20840-55.

42. Nagajyothi PC, Muthuraman P, Tettey CO. In vitro anticancer activity of eco-friendly synthesized ZnO/Ag nanocomposites. Ceram Int 2021;47:34940-8.

43. Patil RS, Kokate MR, Shinde DV, et al. Synthesis and enhancement of photocatalytic activities of ZnO by silver nanoparticles. Spectrochim Acta A Mol Biomol Spectrosc 2014;122:113-7.

44. Welegergs GG, Gebretinsae HG, Tsegay MG. Spectrally selective single layered Ag@ CuO nanocermet coatings for photothermal application: green synthesis method. Opt Mater 2023;135:113247.

45. Agustina TE, Handayani W, Imawan C, editors. The UV-VIS spectrum analysis from silver nanoparticles synthesized using Diospyros maritima blume. Leaves extract. 3rd KOBI Congress, International and National Conferences (KOBICINC 2020); 2021: Atlantis Press.

46. Singh RP, Shukla VK, Yadav RS. Biological approach of zinc oxide nanoparticles formation and its characterization. Adv Mater Lett 2011;2:313-7.

47. Hosny M, Fawzy M, Eltaweil AS. Green synthesis of bimetallic Ag/ZnO@Biohar nanocomposite for photocatalytic degradation of tetracycline, antibacterial and antioxidant activities. Sci Rep 2022;12:7316.

48. Ramyadevi J, Jeyasubramanian K, Marikani A, et al. Copper nanoparticles synthesized by polyol process used to control hematophagous parasites. Parasitol Res 2011;109:1403-15.

49. Akhir RM, Harrum WMW, Buniyamin I. Enhanced structural and morphological properties of ZnO nanorods using plant extract-assisted solution immersion method. Mater Today Proc 2022;48:1855-60.

50. Zhang KX, Wen X, Yao CB, et al. Synthesis, structural and optical properties of silver nanoparticles uniformly decorated ZnO nanowires. Chem Phys Lett 2018;698:147-51.

51. Minhas LA, Mumtaz AS, Kaleem M. Green synthesis of zinc oxide nanoparticles using Nostoc sp. and their multiple biomedical properties. Catalysts 2023;13:549.

52. Anand GT, Renuka D, Ramesh R, et al. Green synthesis of ZnO nanoparticle using Prunus dulcis (Almond Gum) for antimicrobial and supercapacitor applications. Surf Interfac 2019;17:100376.

53. Botcha S, Prattipati SD. Callus extract mediated green synthesis of silver nanoparticles, their characterization and cytotoxicity evaluation against MDA-MB-231 and PC-3 cells. BioNanoScience 2020;10:11-22.

54. Mahmood RI, Kadhim AA, Ibraheem S, et al. Biosynthesis of copper oxide nanoparticles mediated Annona muricata as cytotoxic and apoptosis inducer factor in breast cancer cell lines. Sci Rep 2022;12:16165.

55. Thirumoorthy G, Balasubramanian B, George JA, et al. Phytofabricated bimetallic synthesis of silver-copper nanoparticles using Aerva lanata extract to evaluate their potential cytotoxic and antimicrobial activities. Sci Rep 2024;14:1270.

56. Alkan H, Cigerci IH, Ali MM, et al. Cytotoxic and Genotoxic Evaluation of Biosynthesized Silver Nanoparticles Using Moringa oleifera on MCF-7 and HUVEC Cell Lines. Plants (Basel) 2022;11.

57. Bozorgpour R, Sheybanikashani S, Mohebi M. Exploring the Role of Molecular Dynamics Simulations in Most Recent Cancer Research: Insights into Treatment Strategies. arXiv preprint arXiv:231019950 2023.

58. Sarani M, Roostaee M, Adeli-Sardou M, et al. Green synthesis of Ag and Cu-doped Bismuth oxide nanoparticles: Revealing synergistic antimicrobial and selective cytotoxic potentials for biomedical advancements. J Trace Elem Med Biol 2024;81:127325.

59. Alnuwaiser MA, Betageri VS, Khan MI, et al. Facile synthesis of silver doped-copper oxide nano materials utilizing areca catechu (AC) leaf extract and their antidiabetic and anticancer studies. J Indian Chem Soc 2022;99:100606.

60. Dubey S, Virmani T, Yadav SK, et al. Breaking Barriers in Eco-Friendly Synthesis of Plant-Mediated Metal/Metal Oxide/Bimetallic Nanoparticles: Antibacterial, Anticancer, Mechanism Elucidation, and Versatile Utilizations. J Nanomater 2024;2024:9914079.

61. Monteiro HP, Rodrigues EG, Amorim Reis AKC, et al. Nitric oxide and interactions with reactive oxygen species in the development of melanoma, breast, and colon cancer: A redox signaling perspective. Nitric Oxide 2019;89:1-13.

62. Akhtar MJ, Ahamed M, Alhadlaq HA, et al. Mitochondrial dysfunction, autophagy stimulation and non-apoptotic cell death caused by nitric oxide-inducing Pt-coated Au nanoparticle in human lung carcinoma cells. Biochim Biophys Acta Gen Subj 2020;1864:129452.

63. Suseela V, Nirmaladevi R, Pallikondaperumal M, et al. Eco-Friendly Preparation of Silver Nanoparticles and Their Antiproliferative and Apoptosis-Inducing Ability against Lung Cancer. Life (Basel) 2022;12.

64. Kaplan Ö, Tosun NG, İmamoğlu R. Biosynthesis and characterization of silver nanoparticles from Tricholoma ustale and Agaricus arvensis extracts and investigation of their antimicrobial, cytotoxic, and apoptotic potentials. J Drug Deliv Sci Technol 2022;69:103178.

65. Katifelis H, Mukha I, Bouziotis P, et al. Ag/Au Bimetallic Nanoparticles Inhibit Tumor Growth and Prevent Metastasis in a Mouse Model. Int J Nanomedicine 2020;15:6019-32.

66. Avula LR, Grodzinski P. Nanotechnology-aided advancement in the combating of cancer metastasis. Cancer Metastasis Rev 2022;41:383-404.

67. Singh AK, Malviya R, Prajapati B, et al. Correction: Singh et al. Nanotechnology-Aided Advancement in Combating the Cancer Metastasis. Pharmaceuticals 2023, 16, 899. Pharmaceuticals (Basel) 2024;17.

68. Noorbazargan H, Amintehrani S, Dolatabadi A, et al. Anti-cancer & anti-metastasis properties of bioorganic-capped silver nanoparticles fabricated from Juniperus chinensis extract against lung cancer cells. AMB Express 2021;11:61.

69. Niznansky L, Osinova D, Kuruc R, et al. Natural Taxanes: From Plant Composition to Human Pharmacology and Toxicity. Int J Mol Sci 2022;23.

70. Tariq L, Bhat BA, Hamdani SS, et al. Phytochemistry, pharmacology and toxicity of medicinal plants. Medicinal and Aromatic Plants: Healthcare and Industrial Applications 2021:217-40.

71. Medici S, Peana M, Pelucelli A, et al. An updated overview on metal nanoparticles toxicity. Semin Cancer Biol 2021;76:17-26.

72. Zhang N, Xiong G, Liu Z. Toxicity of metal-based nanoparticles: Challenges in the nano era. Front Bioeng Biotechnol 2022;10:1001572.

73. Zhao H, Wu L, Yan G, et al. Inflammation and tumor progression: signaling pathways and targeted intervention. Signal Transduct Target Ther 2021;6:263.

74. Piotrowski I, Kulcenty K, Suchorska W. Interplay between inflammation and cancer. Rep Pract Oncol Radiother 2020;25:422-7.

75. Villalobos Gutierrez PT, Munoz Carrillo JL, Sandoval Salazar C, et al. Functionalized Metal Nanoparticles in Cancer Therapy. Pharmaceutics 2023;15.

76. Xia K, Yamaguchi K, Suzuki K. Recent Advances in Hybrid Materials of Metal Nanoparticles and Polyoxometalates. Angew Chem Int Ed Engl 2023;62:e202214506.

77. Liu F, Chen H, Deng D, et al. An ultrasensitive immunosensor based on cellulose nanofibrils/polydopamine/Cu-Ag nanocomposite for the detection of AFP. Bioelectrochemistry 2022;147:108200.

78. Abdelkawi A, Slim A, Zinoune Z, et al. Surface modification of metallic nanoparticles for targeting drugs. Coatings 2023;13:1660.

79. Bandyopadhyay A, Das T, Nandy S, et al. Ligand-based active targeting strategies for cancer theranostics. N-S Arch Pharmacol 2023;396:3417-41.